Reprinted from the Journal of the American Ceramic Society, Vol. 68, No. 11, November 1985.
Copyright 1985 by The American Ceramic Society

Microstructure-Strength Properties in Ceramics: II, Fatigue Relations

ROBERT F. COOK,*,# BRIAN R. LAWN,* and CAROLYN J. FAIRBANKS*

Center for Materials Science, National Bureau of Standards, Gaithersburg, Maryland 20899

The study of crack-size effects in aluminas and other selected ceramics in Part I is here extended to dynamic fatigue properties. Controlled flaws are used to measure the fatigue response in the large-crack (indentation-controlled) and small-crack (microstructure-controlled) regions. It is demonstrated that the "microstructural driving forces" responsible for the *R*-curve behavior are readily accommodated into existing indentation fracture theories of fatigue strengths. The modified theory provides well-defined solutions for the strengths in terms of stressing rate and indentation load. Two load-invariant quantities, relating to the exponent and coefficient in an assumed power-law crack velocity function, are sufficient to define the entire data set for a given material, at all stressing rates and loads. This is demonstrated graphically by reducing such data sets onto universal fatigue diagrams. The data for sapphire do not coincide with those for the polycrystalline aluminas, suggesting again that it is the grain-boundary structure which holds the key to the fracture properties in the latter. From the standpoint of reliability, the study emphasizes the need to account for microstructural effects when extrapolating to the domain of naturally occurring flaws. In this context, the adjustable quantities obtained from the dynamic fatigue data fits emerge as appropriate design parameters.

I. Introduction

In PART I of this two-part series we developed a fracture mechanics analysis for *equilibrium* cracks in "coarse-grained" ceramics.[1] It was asserted there that the material microstructure can be a significant factor in determining the fracture properties, by contributing to the net crack driving force at the local level. This contribution is manifest as a progressive reduction in the apparent toughness as the crack size reduces toward grain dimensions (*R*-curve). In view of the strength of the effect in some of the materials studied, it becomes pertinent to ask whether *non-equilibrium*, or fatigue, properties are similarly microstructure sensitive. Do the same restrictions as described in Part I apply when extrapolating large-scale crack velocity data to the practical domain of microscopic flaws?

In appealing to the literature for evidence bearing on this last question, one is faced with limited and sometimes conflicting experimental data. Most of this evidence takes the form of discrepancies between evaluations of the exponent n in an assumed (empirical) power-law crack-velocity/stress-intensity-factor equation at opposite ends of the crack-size spectrum, at the macroscopic end by direct measurement of growth rates in "conventional" test specimens (e.g., double-cantilever beam, double torsion), and at the microscopic end by measuring the slopes of "dynamic fatigue" (strength vs stressing rate) curves for specimens with as-finished (usually machined) surfaces. Pletka and Wiederhorn[2] have provided a comprehensive compilation of existing data up to 1982, including their own, in which the variability that can bedevil results obtained by different techniques (or worse, by different workers) is all too apparent. This variability notwithstanding, Pletka and Wiederhorn were led to conclude that, for a given material, n values from strength curves tend to be systematically lower than their direct-measurement counterparts. They recognized that some kind of crack-microstructure interaction could be responsible for the effect, but made no suggestion as to how such an interaction might be incorporated into a fracture mechanics formalism.

In the light of this background of restricted evidence, the indentation flaw technique presents itself as a unique opportunity to investigate size effects in fatigue properties. The power of this technique in fatigue analysis has already been extensively demonstrated for *homogeneous* materials.[3–12] From the standpoint of a strength formulation, one has only to fold in an appropriate crack velocity function with the stress intensity factor for radial cracks to obtain the rate dependency. The approach then offers two major advantages to the experimentalist. First, as with our investigation into the toughness characteristics,[1] we have the facility to vary the contact load, and thereby bridge the gap between macroscopic and microscopic fracture domains. Thus in a study on silicate glasses[7] it was possible to confirm that a single crack velocity law can be used to fit dynamic fatigue data over a load range of some 3 orders of magnitude (embracing the size region characteristic of natural flaws). Second, quantitative evaluations of the crack velocity constants may be obtained directly from the fatigue data fits. Again in silicate glasses, *provided* due allowance is made for residual contact stresses about the flaws, such evaluations agree with those obtained independently from large-scale crack specimens.[3,7] It would seem to require one small step, that of reworking the fracture mechanics analysis with the *modified* stress intensity factor from Part I, i.e., with the "grain-localized" term included, to allow for extension of the technique to the microstructure-sensitive materials of interest here.

In this paper we shall pursue such a course in an effort to develop a suitably generalized dynamic fatigue relation. Attention in this development will focus on the role of the microstructural driving forces in the fatigue susceptibility. In view of our intimation above that the residual contact stresses have an important influence on the evaluation of this susceptibility, should we not expect an equally important influence from the microstructural component? The stress intensity factors for these two contributions are, after all, assumed to have the same crack-size dependence.[1] Our analysis will show that the two contributing factors are in fact indistinguishable in their effect on the predicted *slopes* of the dynamic fatigue curves; the "apparent" crack velocity exponent (i.e., the exponent we would determine if we were to make no allowance for these additional factors) is independent of whether the indentation flaws are in the high-load (indentation-controlled) or low-load (microstructure-controlled) region. We shall examine this predicted behavior by comparison with dynamic fatigue data on some of the materials listed in Part I, using water as the test environment in each case. Some recent, complementary data on glass-ceramics by other workers[13] will also be considered in this connection. In making these comparisons between theory and experiment, some general trends within material classes (particularly alumina) will be noted, pointing the way once more to the importance of grain-boundary structures. The implications of the results concerning reliability predictions in ceramics will be given due attention, with particular emphasis on the potential dangers of omitting microstructural terms from the fracture mechanics analysis when using crack velocity data to predict component lifetimes.

Received February 28, 1985; revised copy received July 29, 1985; approved August 9, 1985.

Supported by the U.S. Air Force Office of Scientific Research. Support for R. F. Cook provided by the NBS Guest Worker Program.

*Member, the American Ceramic Society.

#Present address: I.B.M., T.J. Watson Research Center, Yorktown Heights, NY 10598.

II. Fracture Mechanics

Following the fracture mechanics analysis in Part I, we begin with the stress intensity factor for radial indentation cracks, allowing now that we shall be dealing with nonequilibrium states. Thus from Eqs. (3) and (5) in Part I we obtain

$$K = \psi\sigma_a c^{1/2} + \chi(P + P^*)/c^{3/2} \tag{1}$$

where c is the characteristic crack dimension, P is the peak indentation load, P^* is an analogous load (real or effective) which incorporates the grain-localized microstructural driving force, σ_a is the applied tensile stress which subsequently takes the system to failure, and ψ and χ are dimensionless parameters. It will be recalled that this equation conveniently contains the provision for systematically describing the transition from indentation-controlled strength behavior at large crack sizes ($P \gg P^*$) to microstructure-controlled behavior at small crack sizes ($P \ll P^*$).

The next step is to introduce an appropriate rate-dependent crack growth condition. In accordance with currently accepted practice in the ceramics fracture testing community, and with our own precedent in the earlier analyses on homogeneous materials,[3–5,7,9] we choose the simple crack velocity function

$$v = v_0(K/K_c^\infty)^n \tag{2}$$

where n and v_0 are material-environment "constants." At the outset we should emphasize that this function is empirically determined; we have no scientific basis for predetermining the constants for any given material system, or indeed for justifying the power-law form of the equation. Moreover, in using the polycrystalline toughness K_c^∞ as a normalizing quantity for the stress intensity factor in Eq. (2), we assume in effect that changes in K_c^∞ are felt in the $v(K)$ response as simple translations along the K axis. While there does appear to be some foundation for this last assumption, in particular from models in which the process responsible for the changes in toughness operates independently of the intrinsic, rate-dependent bond-rupture micromechanism,[14] the validity of our crack "law" must ultimately be measured in the success in fitting experimental fatigue data.

The strength testing procedure of special interest here is that of so-called dynamic fatigue, in which the rate of applied stressing is held fixed

$$\dot{\sigma}_a = \sigma_a/t = \text{constant} \tag{3}$$

up to the point of failure. The object of the fracture mechanics exercise now is to solve Eqs. (1) to (3) simultaneously to determine the fatigue strength σ_f as a function of the independent test variables, $\dot{\sigma}_a$ and P.

Our strategy in solving for this fatigue function is to seek a way of reducing the master differential equation which culminates from the above expressions into a form equivalent to that for the special case $P^* = 0$, $K_c^\infty = K_c$, i.e., for zero microstructural effect. Then we can simply draw from the well-documented analytical solutions for homogeneous materials.[5,9] A key step in these earlier analyses was to rewrite the master equation in normalized form, using the critical applied stress σ_m and corresponding crack size c_m at equilibrium failure to define a convenient reference state. From Part I, Eqs. (6) and (8), we have the analogous, generalized quantities

$$c_m = [3\chi(P + P^*)/\psi\sigma_m]^{1/2} \tag{4a}$$

$$\sigma_m = 3K_c^{\infty\,4/3}/4^{4/3}\psi\chi^{1/3}(P + P^*)^{1/3} = \sigma_m^Q P^{*1/3}/(P + P^*)^{1/3} \tag{4b}$$

where σ_m^Q is the asymptotic low-load strength limit in the microstructure-controlled region. If now we introduce the earlier normalizing scheme,[5] defined by the reduced variables

$$S_a = \sigma_a/\sigma_m \tag{5a}$$

$$C = c/c_m \tag{5b}$$

$$T = tv_0/c_m \tag{5c}$$

then Eqs. (1) to (3) combine to give the dimensionless master equation

$$dC/dT = (3\dot{S}_a C^{1/2}T/4 + 1/4C^{3/2})^n \tag{6}$$

where $\dot{S}_a = S_a/T$ = constant. This is precisely the same differential equation as before;[5,9] all we have had to do to get to this common starting point is to redefine our reference state, Eq. (4), to allow for the additional microstructural influence.

The solution to Eq. (6) is obtained in accordance with initial (stable) and final (unstable) equilibrium states: $C = C_0 \approx 0.4$ (cf. Eqs. 6 and 7, Part I) at $T = 0$; $C = C_f$ (defined by requirement $dK/dc > 0$, $K = K_c^\infty$) at $T = T_f = S_f/S_a$.[9] This solution has a familiar power-law form

$$S_f = (\Lambda'\dot{S}_a)^{1/(n'+1)} \tag{7}$$

in the fatigue region $S_f < S_m = 1$, where

$$n' = 3n/4 + 1/2 \tag{8a}$$

$$\Lambda' = (2\pi n')^{1/2} \tag{8b}$$

In conjunction with Eqs. (5) and (8), Eq. (7) may now be denormalized to give ($\sigma_f < \sigma_m$)

$$\sigma_f = (\lambda'\dot{\sigma}_a)^{1/(n'+1)} \tag{9}$$

with the intercept term

$$\lambda' = (2\pi n')^{1/2}\sigma_m^{n'}c_m/v_0 \tag{10}$$

As previously noted,[5,9] Eq. (9) gives exactly the same linear plot in logarithmic coordinates as does the corresponding dynamic fatigue relation for "Griffith" flaws (i.e., flaws free of *any* extraneous influence, other than that of the applied stressing), except that the slopes and intercepts are modified. Thus, whereas for Griffith flaws the "apparent" crack velocity exponent n' identifies with the "true" value n, with the more general case represented by Eq. (8*a*) the apparent value is significantly reduced. We may note in passing that this latter discrepancy is consistent with the experimental observations of Pletka and Wiederhorn mentioned in Section I.

It is useful to consider the above formulation more closely in terms of the specific goals of the present study, and thence to introduce some minor modifications. A major goal, of course, is to investigate how the fatigue response depends on indentation load P, particularly on traversing the transition point at P^*. The first thing that is immediately clear, from Eqs. (8*a*) and (9), is that the slopes should be completely independent of load. (There is a qualification that we ought to make in connection with this statement, however, which is that the constancy of n' is contingent on the residual contact stress contribution remaining at "full strength";† if this contribution were somehow to be removed, e.g., by annealing, or polishing away a portion of the indented surface, then n' would revert to the value n on passing into the high-load region.[3]) The intercepts, on the other hand, will depend strongly on load, since the reference quantities σ_m and c_m which appear in Eq. (10) are themselves load dependent (Eq. (4)). Actually, there is some advantage in retaining σ_m explicitly in the formulation, both because it is easily measured experimentally (Part I) and because it sets an upper bound to the fatigue strength. However, c_m is not such a conveniently accessible experimental quantity, particularly in view of the geometrical complexities that characterize the crack pattern in coarse-grained microstructures,[1,15] so we insert Eq. (4*a*) into Eq. (10) to eliminate it. Equation (9) may now be written in the form (at $\sigma_f < \sigma_m$)

$$\sigma_f = \sigma_m\{\eta'[(P + P^*)/\sigma_m^3]^{1/2}\dot{\sigma}_a\}^{1/(n'+1)} \tag{11a}$$

or alternatively, in combination with Eq. (4*b*), as

---

†A measure of this "full strength" is given by the requirement $c_0' < c_m$ (Refs. 3, 5, and 9): in practice, c_m (Eq. (6) in Part I) can diminish by virtue of any reduction in the residual stress intensity, as characterized by χ; at the same time, the initial crack size c_0' immediately prior to strength testing may substantially exceed the equilibrium size c_0 (Eq. (7) in Part I) owing to postindentation slow crack growth.

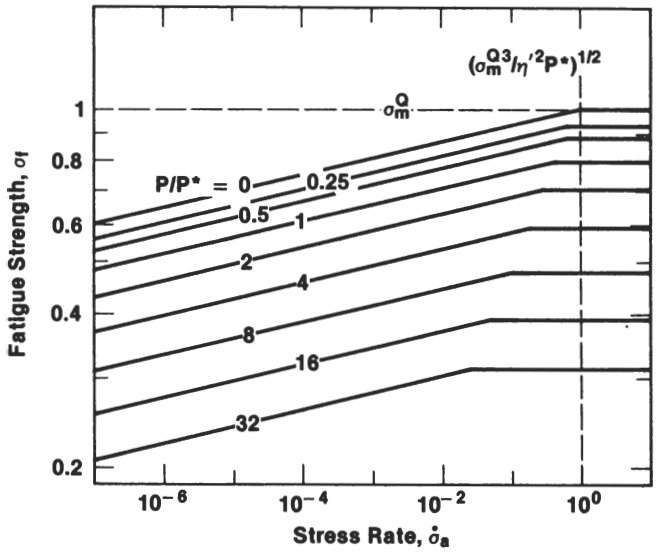

Fig. 1. Normalized plots of fatigue strength vs stressing rate at different indentation loads. Solid lines represent Eq. (11) for $n = 39.3$ ($n' = 30$); broken line represents upper bound of inert strength. Note how plots bunch up as load reduces into microstructure-controlled region ($P < P^*$).

$$\sigma_f = \sigma_m^Q[P^*/(P + P^*)]^{(n'-2)/3(n'+1)} \{\eta'[P^*/(\sigma_m^{Q3})]^{1/2}\dot{\sigma}\}^{1/(n'+1)} \tag{11b}$$

where η' is a function of crack velocity parameters, independent of load

$$\eta' = (6\pi n'\chi/\psi v_0^2)^{1/2} \tag{12}$$

Plots of Eq. (11*b*) are shown in Fig. 1 for different values of P/P^*. The diminishing sensitivity to indentation load on entering the microstructure-controlled region ($P < P^*$) is apparent in these plots.

As we shall see later, our formalism is convenient for data comparison at different toughnesses as well as at different loads; we recall from Eq. (4*b*) that σ_m depends on K_c^∞ as well as on P. Hence, by plotting σ_f/σ_m vs $[(P + P^*)/\sigma_m^3]^{1/2}\dot{\sigma}_a$ in accordance with Eq. (11*a*) we can in principle reduce all fatigue data for a given material-environment system, *including* composition variants within the material class, onto a universal plot, provided n' and η' remain constant. This last proviso holds if the basic crack velocity parameters n and v_0 remain constant (see Eqs. (8*a*) and (12)), consistent with the appearance of K_c^∞ as a scaling quantity in Eq. (2). Put another way, the observation that data from different materials *do* plot onto a universal curve may be taken as implying a certain commonality in the intrinsic bond-rupture processes which control the crack rate.

III. Experimental Procedure

The materials used for the fatigue study were those of the aluminas, barium titanates, and glass-ceramics listed in Part I available to us in sufficient quantities. The specimen preparation and test procedure was much the same as before,[1] with the following modifications.

First, the Vickers indentation loads for each complete dynamic fatigue run were chosen in accordance with the strength of the *R*-curve behavior for each given material. Thus, for those materials with pronounced low-load plateaus in the inert-strength response (Part I), the object was to sample both the indentation-controlled and the microstructure-controlled regions with values of P on either side of P^*. Where such plateaus were not so apparent, a single indentation load was deemed sufficient. Again, these choices were subject to the restrictions mentioned previously,[1] that the indentations should not be dominated by natural flaws at low P or be accompanied by excessive chipping at high P. With one particular material, the VI1 alumina, some specimens were left unindented as controls.

Second, and most important, the strength tests themselves were run in distilled water as a "standard" environment, replacing the oil used for the inert tests. Each failure was obtained at a fixed stressing rate. The range of stressing rates available to us was somewhere between 10^{-3} to 10^5 MPa·s^{-1}, depending on the specific test geometry (again making use of a piezoelectric load cell to monitor the faster breaks[6]).

Care was taken, as usual, to confirm that failure did indeed initiate from the contact sites. The few exceptions that did occur were excluded from the data base.

IV. Results

The results of the dynamic fatigue runs for the aluminas, barium titanates, and glass-ceramics are shown in Figs. 2 to 4. Each data point in these plots represents the mean and standard deviation (in logarithmic coordinates) of 8 to 10 breaks from indentation flaws at the appropriate stressing rate and load. The horizontal broken lines at right in the plots indicate the upper bound strengths for each load used, taken from the corresponding $\sigma_m(P)$ data base in the preceding inert-strength study (see Figs. 4 to 6, Part I). The value of P^* for each material (see Table II, Part I) is likewise indicated, as a reminder of where the individual sets of data lie in the spectrum of indentation vs microstructure control. Least-squares best fits in accordance with Eq. (11*a*), treating n' and η' as adjustable parameters, are shown as the straight lines through the data sets. Table I lists the values of these parameters.

There are certain features in these results which deserve elaboration. For a start, notwithstanding the linear fitting procedure used to analyze the data, there appears to be some real curvature in the dynamic fatigue responses in Figs. 2 to 4. This only serves to amplify the misgivings hinted at earlier concerning the empirical power-law form of the crack velocity function in Eq. (2). More significantly, however, taking n' and η' in Table I at face value, we note that there exist apparent consistencies in the listed fatigue parameters. This is particularly so at different loads (where applicable) for any given material, regardless of whether P is greater or less than P^*. Such consistencies may be seen to even greater effect by replotting the points in Figs. 2 to 4 onto graphs of σ_f/σ_m vs $[(P + P^*)/\sigma_m^3]^{1/2}\dot{\sigma}_a$, as advocated in Section II. This is done in Figs. 5 to 7 for the aluminas, barium titanates, and glass-ceramics, respectively. Apart from the sapphire results in Fig. 5, there seems to be some tendency for all the data points in each diagram to plot onto universal curves, at least to within experimental scatter bands (omitted for some of the materials represented in these graphs for sake of clarity).

This apparent tendency to universality gives us confidence in making data extrapolations: first, in using large-scale crack velocity data to predict the fatigue response of microscopic flaws; second (although with more reservation), in foreshadowing the fatigue properties of new member materials in a group. The prerequisite for such extrapolations is knowledge of the function $\sigma_m(P, P^*)$ for a specific material, underscoring once more the importance of establishing the equilibrium toughness (*R*-curve) parameters as a reference base.

Pointed mention was made above of sapphire as the clearest exception to universality in the fatigue behavior for the aluminas (Fig. 5). This result is consistent with the difference in fracture mode reported in Part I, from bulk cleavage in the single crystal to predominantly intergranular cracking in the polycrystals. (As mentioned also in Part I, similar distinctions were not possible in the barium titanates and glass-ceramics, owing to unavailability of appropriate monocrystal or matrix reference materials.) It is therefore not too surprising that sapphire should show such distinctive fatigue behavior, for the bond chemistry which governs the intrinsic crack growth response is surely different within the bulk structure in comparison to that at a grain boundary. What is perhaps surprising is that all the polycrystalline aluminas tested should show an apparent *similarity* in behavior, notwithstanding the spread of n' values evident in Table I. The implication is that the

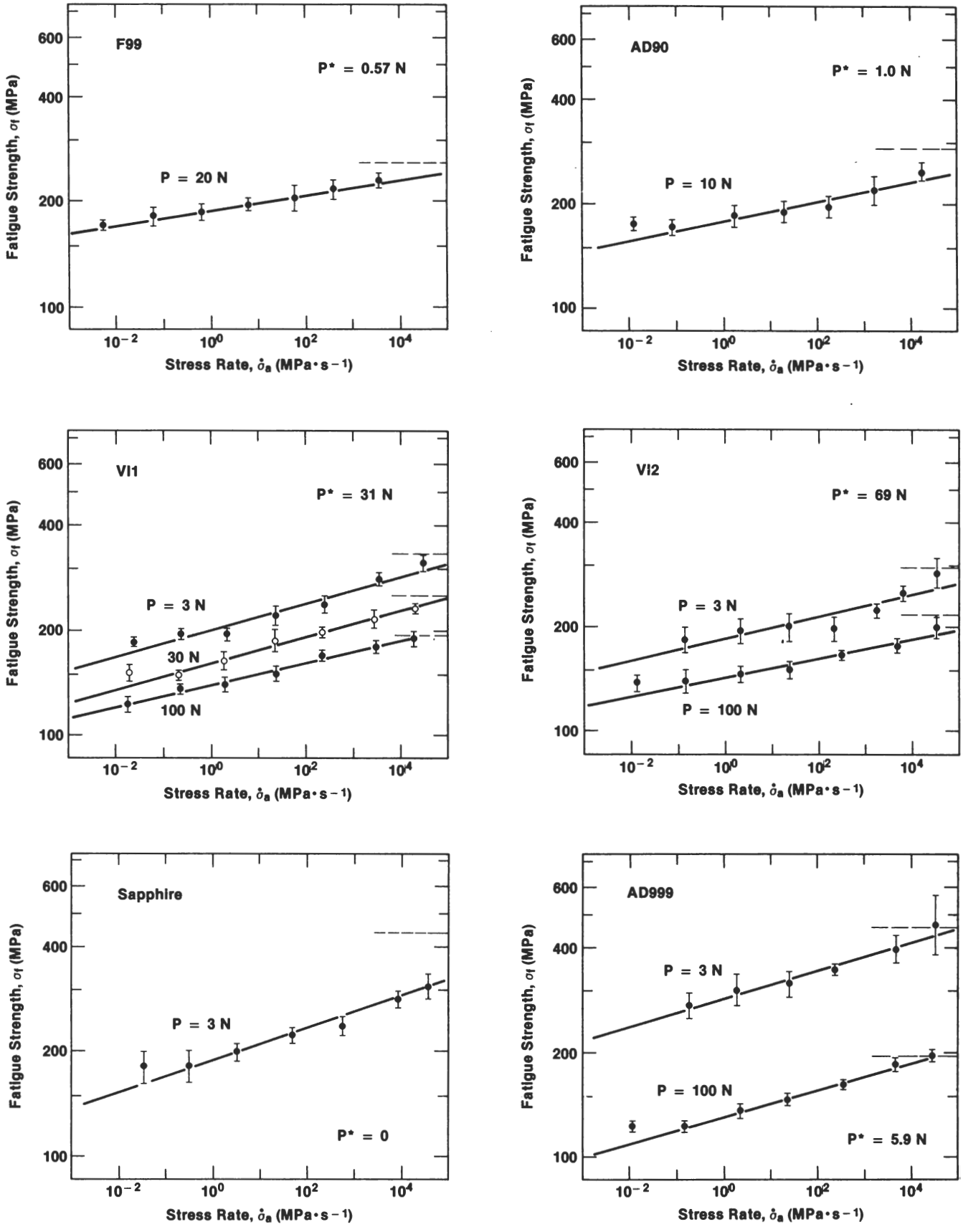

Fig. 2. Dynamic fatigue plots for aluminas in water at selected indentation loads.

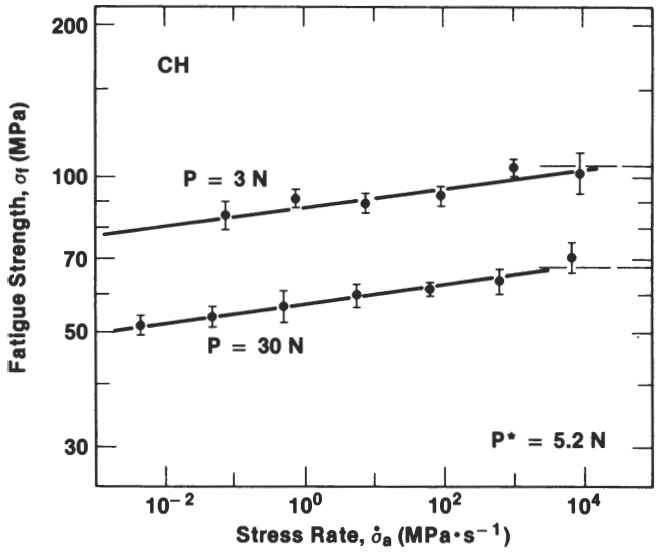

Fig. 3. Dynamic fatigue plots for barium titanate ceramic in water at selected indentation loads.

same microstructural influences which play such a critical role in determining the *R*-curve response are not quite so strongly felt in the grain-interface/environment chemistry.

Lastly, to confirm that the above analysis does indeed extend to naturally occurring flaws, a dynamic fatigue run was made on unindented VI1 alumina controls. This particular material was selected for its pronounced inert-strength plateau, so that the flaw population could be guaranteed as truly intrinsic to the microstructure (see Part I). The results of this run are shown in Fig. 8. The data points are plotted as before; but the straight line now represents a *prediction* from Eq. (11*b*), at $P = 0$, using appropriate values of n' and η' from Table I (averaged over the three loads listed) along with σ_m^Q and P^* from Table II in Part I. The level of agreement between theory and experiment in this figure would appear to reinforce the conviction that we are dealing with general phenomena here.

V. Discussion

In this study we have developed a nonequilibrium fracture mechanics formalism, whereby the same microstructural driving force term responsible for the *R*-curve behavior in Part I is incorporated into dynamic fatigue relations. The essential predictions of this formalism are shown to be consistent with data on test specimens containing indentation flaws. Most importantly, the influence of the microstructure is reflected in the slope of the fatigue strength vs stressing rate plot. In this regard, the influence is identical with that of the residual contact term: a reduction of close to ¾ in the fatigue susceptibility exponent n' relative to the value n that one would infer from the more conventional analysis based on "Griffith-like" flaws (see Eq. (8*a*)). Thus the discrete grain structure is felt as a deleterious force in the nonequilibrium as well as the equilibrium strength properties of ceramics.

How widespread is this effect? It might be argued that many, if not most, flaw populations may never experience the crack stabilizing forces embodied in the $c^{-3/2}$ term in Eq. (1). In response to this, we need to emphasize the following point: if the condition $n' = n$ is to hold for natural flaws, then *both* the microstructural and the residual contact forces (or, indeed, any other stabilizing forces) must be inoperative. Such an ideally benign flaw state could be extremely difficult to achieve. We have already seen from the inert-strength plateaus in Part I that a strong, even dominant, microstructural influence is evident in the natural flaw populations of many ceramics. The agreement between the dynamic fatigue data for the as-received VI1 alumina and the theoretical

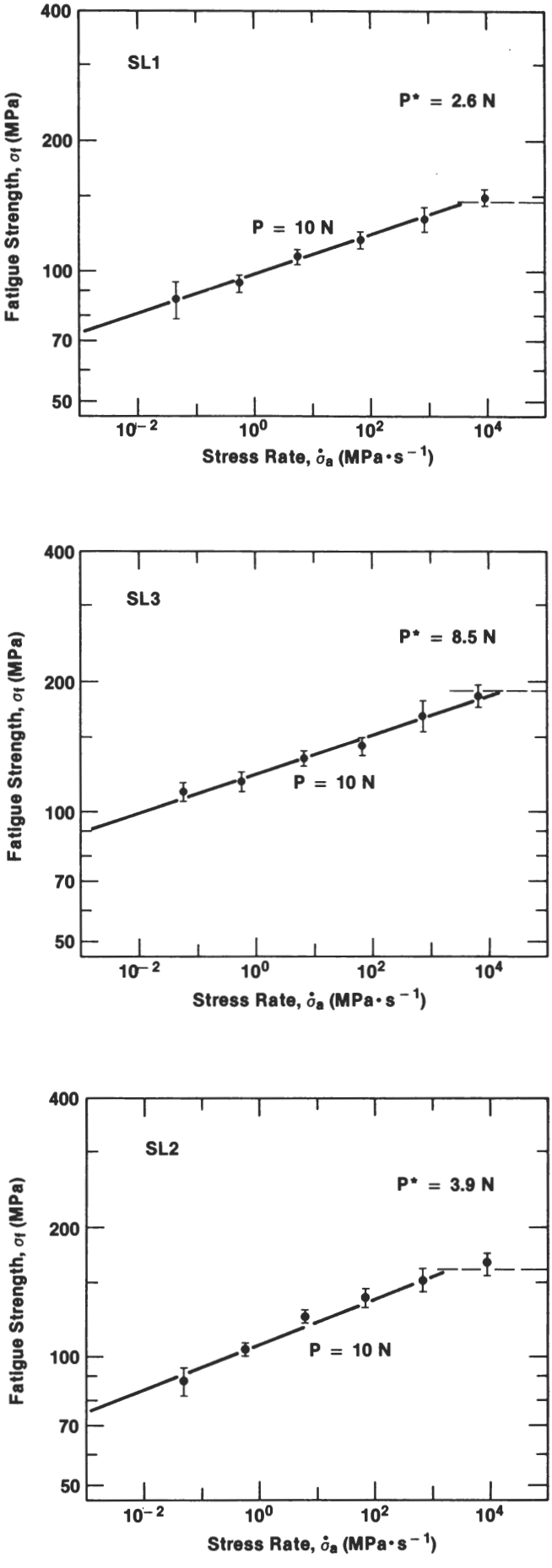

Fig. 4. Dynamic fatigue plots for glass-ceramics in water at selected indentation load.

Table I. Fatigue Parameters of Test Materials*

Material		P (N)	n'	log η' (η' in $m^{-1}\cdot s$)
Al_2O_3	Sapphire	3	20.9	−1.32
	AD999	3	23.6	1.47
	AD999	100	24.8	0.94
	AD90	10	34.2	−1.21
	VI1	3	25.0	0.34
	VI1	30	25.6	0.46
	VI1	100	30.8	0.83
	VI2	3	29.7	−0.60
	VI2	100	35.4	−1.27
	F99	20	45.1	−0.62
$BaTiO_3$	CH	3	54.6	1.30
	CH	30	52.4	1.26
Glass-ceramic	SL1	10	21.0	1.99
	SL2	10	18.2	2.62
	SL3	10	21.2	1.48

*Evaluated in conjunction with inert-strength parameters from Table II of Part I.

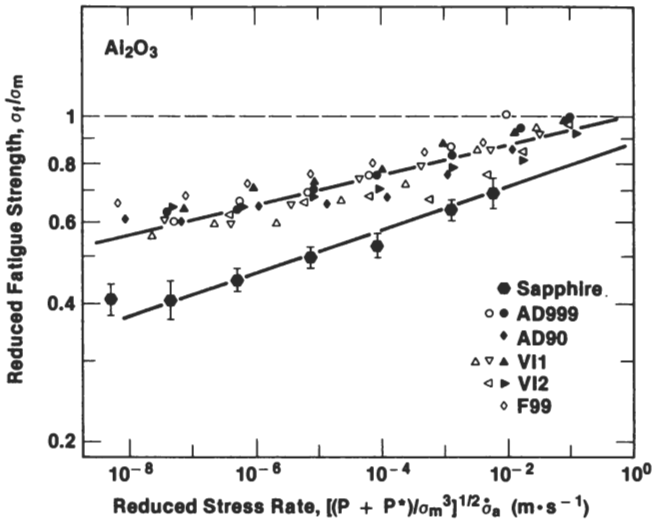

Fig. 5. Replot of data for alumina/water in Fig. 2 in accordance with scheme for producing universal fatigue curves. Upper line represents average over all n' and η' parameters listed for polycrystalline aluminas in Table I; lower line represents sapphire parameters only.

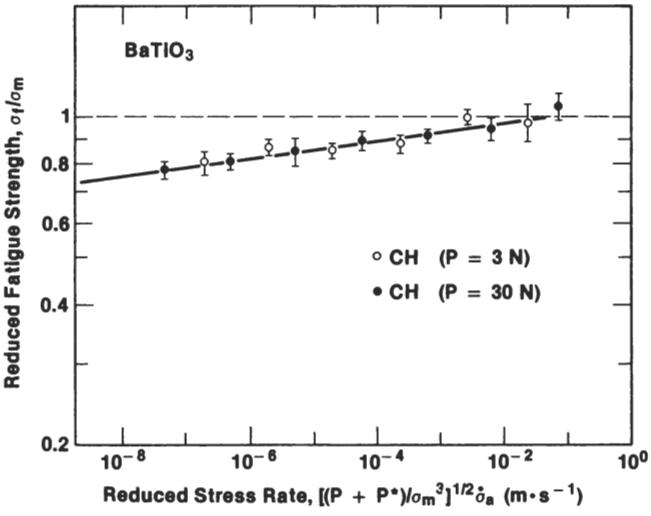

Fig. 6. Universal curve for barium-titanate/water, replotted from data in Fig. 3. Line represents average over n' and η' parameters listed at different loads in Table I.

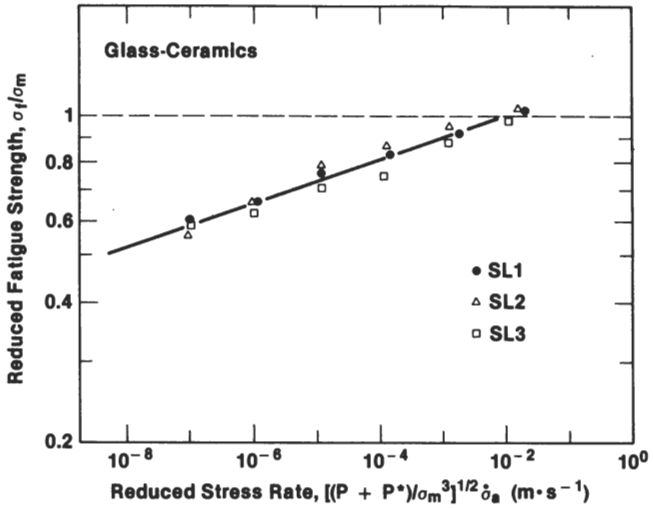

Fig. 7. Universal curve for glass-ceramics/water, replotted from data in Fig. 4. Line represents average over n' and η' parameters listed for glass-ceramics in Table I.

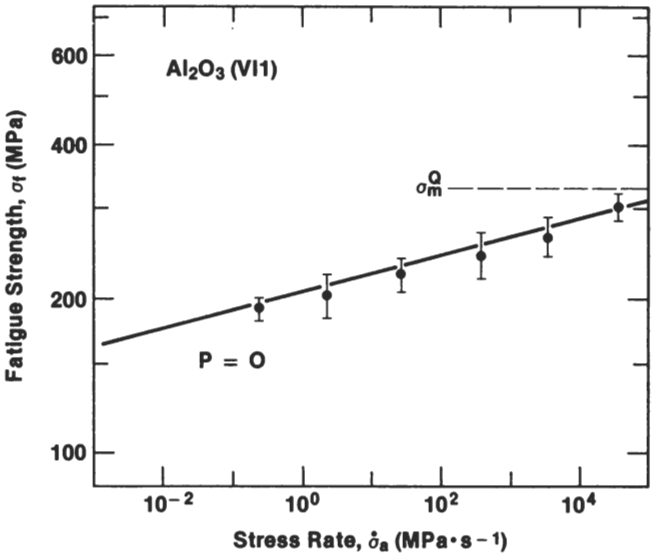

Fig. 8. Dynamic fatigue curve for *un*indented VI1 alumina in water. Solid line is prediction from indentation analysis, in zero-load limit of Eq. (11).

prediction from the indentation analysis (in the zero-load limit) in Fig. 8 is a reflection of this dominant influence. Again, many natural flaws arise from handling or machining damage and are thereby subject to the same kind of residual contact effects as the indentations described here.[16] It is, in fact, common practice to prepare ceramic test specimens by machining their surfaces. The systematically low n' values associated with the fatigue strength data in the Pletka and Wiederhorn survey[2] (see Section I) are testament to the almost ubiquitous presence of such sources of flaw stabilization in the finished ceramics component.

Let us now address specifically the issue of crack size effects, to which we have attached such importance in our two-part study. In Part I we saw that crack size, or more directly indentation load, was a critical factor in the controlling equilibrium fracture parameter, i.e., the (apparent) toughness. Following our discussion in the previous two paragraphs, we find that the important *non*equilibrium fracture parameter, the fatigue susceptibility exponent, is independent of indentation load (subject to the quali-

fication indicated in Section II, that the residual contact force should remain fully operational, i.e., free of relaxation effects). Thus dynamic fatigue functions at different P plot as a family of parallel lines, in the manner of the schematic representation of Eq. (11*b*) in Fig. 1. This parallelism is evident in the actual data plots in Figs. 2 to 4 for those materials tested at more than one load, regardless of the value of P relative to P^*. Where the load dependence *is* apparent, of course, is in the composite intercept term in Eq. (11*b*), as manifested by the translational shifts in the fatigue plots. The self-consistency of η' values obtained at different loads for a given material (where applicable) in Table I, and the corresponding universality in the reduced plots of Figs. 5 to 7, indicate that Eq. (11*b*) properly accounts for this load dependence. Corollary to this self-consistency is the implied "correctness" of the $c^{-3/2}$ dependence of the microstructural and residual contact stress intensity factor contributions in Eq. (1), reinforcing further the conclusions already drawn in Part I.

In this context of size effects in fatigue data, specific mention may be made of some recently reported work by others[13] on the VPI glass-ceramics detailed in Part I. These workers found the slopes of dynamic fatigue curves to remain independent of load, as we have done, down to the point at which the crack size becomes comparable with the crystallite size. At this extreme low-load limit the slope appeared to show a systematic change, toward a value more representative of the material matrix. Thus, unlike the alumina, where the fatigue relation Eq. (11*b*) holds down to the zero-load limit (see Fig. 8), there is the indication in the glass-ceramics that the crack velocity function becomes sensitive to the two-phase structure in the microflaw region. It is interesting to recall from Part I that these same glass-ceramics showed no such discontinuity in their toughness characteristics at low loads (presumably because the toughness represents an *averaged* crack resistance over an extensive, stable precursor growth stage).

There are some fundamental questions that we may raise in connection with the results summarized in the universal plots of Figs. 5 to 7. What are the key features of the material microstructure, particularly at the grain-boundary interfaces, that determine the crack growth kinetics? How is it that these features appear to remain somewhat insensitive to those same microstructural details which so dramatically influence the equilibrium toughness (R-curve) behavior (Part I)? We have suggested that there are some physical grounds for believing that the intrinsic bond-rupture processes may operate somewhat independently of the subsidiary processes responsible for toughness variations.[14] If so, how may we reconcile such behavior with the empirical crack velocity formula in Eq. (2)? Indeed, does Eq. (2) contain the essence of the true $v(K)$ relationship? Scientific issues such as these have been obscured in the past by our preoccupation with the demands of engineering design.

It is appropriate in connection with this last oblique reference to engineering design to consider our fracture mechanics analysis in terms of fatigue strength predictions in the practical domain. First, the analysis provides us with a sound basis for extrapolating results from the large to the small crack-size regions. As we see from Eq. (11*b*), a dynamic fatigue run at constant P allows us to predetermine the corresponding response at a different P, provided that the inert strength parameters σ_m^Q and P^* are established first. For those especially deleterious cases with strong R-curve behavior, this extrapolation can be taken to its extreme limit at $P = 0$ to predict the natural flaw response. Indeed, the same extrapolation can be made without a reference dynamic fatigue run if the macroscopic crack velocity function, Eq. (2), is known, using Eqs. (8*a*) and (12) as transformation relations to evaluate the slope and intercept parameters in Eq. (11*b*). Second, if one were prepared to accept the universality in Figs. 5 to 7 in good faith, one could in principle extrapolate the results to new materials within a given composition type, provided again that the inert strength function $\sigma_m(P, P^*)$ could be determined for this new material. Of course, this is a much more risky extrapolation, for there can be no guarantee that all material variants will be as "well-behaved" as those we happen to have selected in our study. Nevertheless, if we have reason to suspect our predictions, a *limited* dynamic fatigue run should be sufficient to restore confidence (or otherwise, as the case may be). And third, the analysis retains all the necessary features of conventional fatigue formulations for extrapolating in time, in particular to the long-lifetime region. Here the limitations lie not so much in the accountability of the microstructural driving forces as in the uncertainties in the crack velocity function, as implied in the previous paragraph. The curvature of the fatigue plots in Figs. 2 to 4 is specially significant in this respect.

VI. Conclusions

(i) The indentation fracture representation of microstructural driving forces in terms of center-loaded penny-crack configurations (Part I) fits experimental dynamic fatigue data over the microscopic-to-macroscopic crack-size spectrum.

(ii) The slope and intercept of the dynamic fatigue plot at a given load can be specified by two parameters (n' and η') which relate directly to the crack velocity exponent and coefficient (n and v_0). These two parameters should be useful in reliability evaluations of a specified material. It is emphasized that the slope and intercept for the indentation flaw are significantly different than for the classical "Griffith" flaw, so that extrapolations which ignore the microstructural effect are subject to large errors.

(iii) Dynamic fatigue data at different indentation loads plot as a family of parallel curves in logarithmic coordinates. Thus the fatigue susceptibility parameter (n') is load independent. On entering the microstructure-controlled region ($P < P^*$), the curves bunch together, indicating a decreasing sensitivity to flaw severity. The fatigue data can be reduced onto a universal curve, using inert-strength parameters (Part I) to define suitable reference states.

(iv) For materials with strong R-curve behavior, the indentation data can be extrapolated to zero load to predict the fatigue response for natural flaws. Agreement between such predictions and actual results on unindented specimens (Fig. 8) confirms that the microstructural influence applies to all flaw types, regardless of origin.

(v) There is a significant disparity between the fatigue data for polycrystal and single-crystal alumina. This suggests that the grain boundary is the controlling element in the microstructural effect, reinforcing the conclusions from the toughness study in Part I.

Acknowledgments: The authors gratefully acknowledge the assistance of D. E. Roberts and B. J. Hockey for assistance in specimen preparation and examination, and D. Heuckeroth and T. L. Baker for obtaining some preliminary data.

References

[1]R. F. Cook, B. R. Lawn, and C. J. Fairbanks, "Microstructure-Strength Properties in Ceramics: I, Effect of Crack Size on Toughness"; this issue, preceding article.

[2]B. J. Pletka and S. M. Wiederhorn, "A Comparison of Failure Predictions by Strength and Fracture Mechanics Techniques," *J. Mater. Sci.*, **17** [5] 1247–68 (1982).

[3]D. B. Marshall and B. R. Lawn, "Flaw Characteristics in Dynamic Fatigue: The Influence of Residual Contact Stresses," *J. Am. Ceram. Soc.*, **63** [9–10] 532–36 (1980).

[4]P. Chantikul, B. R. Lawn, and D. B. Marshall, "Micromechanics of Flaw Growth in Static Fatigue: Influence of Residual Contact Stresses," *J. Am. Ceram. Soc.*, **64** [6] 322–25 (1981).

[5]B. R. Lawn, D. B. Marshall, G. R. Anstis, and T. P. Dabbs, "Fatigue Analysis of Brittle Materials Using Indentation Flaws: I," *J. Mater. Sci.*, **16** [10] 2846–54 (1981).

[6]R. F. Cook, B. R. Lawn, and G. R. Anstis, "Fatigue Analysis of Brittle Materials Using Indentation Flaws: II," *J. Mater. Sci.*, **17** [4] 1108–16 (1982).
[7]T. P. Dabbs, B. R. Lawn, and P. L. Kelly, "A Dynamic Fatigue Study of Soda-Lime Silicate and Borosilicate Glasses Using Small-Scale Indentation Flaws," *Phys. Chem. Glasses*, **23** [2] 58–66 (1982).
[8]B. R. Lawn; pp. 1–25 in Fracture Mechanics of Ceramics, Vol. 5. Edited by R. C. Bradt, A. G. Evans, D. P. H. Hasselman, and F. F. Lange. Plenum, New York, 1983.
[9]E. R. Fuller, B. R. Lawn, and R. F. Cook, "Theory of Fatigue for Brittle Flaws Originating from Residual Stress Concentrations," *J. Am. Ceram. Soc.*, **66** [5] 314–21 (1983).
[10]H. Multhopp, R. F. Cook, and B. R. Lawn, "Universal Fatigue Curves for Ceramics Using Indentation Flaws," *J. Mater. Sci. Lett.*, **2** [11] 683–84 (1983).
[11]R. F. Cook and B. R. Lawn; pp. 22–42 in Methods for Assessing the Structural Reliability of Brittle Materials. Edited by S. W. Freiman and C. M. Hudson. *ASTM Spec. Publ.*, **No. 844** (1984).
[12]B. R. Lawn, D. B. Marshall, and T. P. Dabbs; to be published in Strength of Glass. Edited by C. J. Kurkjian. Plenum, New York.
[13]S. Baskaran, S. B. Bhaduri, and D. P. H. Hasselman, "Effect of Crystallites on Subcritical Crack Growth and Strain-Rate Sensitivity of Strength of Cordierite Glass-Ceramics," *J. Am. Ceram. Soc.*, **68** [3] 112–19 (1985).
[14]B. R. Lawn, "Physics of Fracture," *J. Am. Ceram. Soc.*, **66** [2] 83–91 (1983).
[15]S. S. Smith and B. J. Pletka; pp. 189–209 in Fracture Mechanics of Ceramics, Vol. 6. Edited by R. C. Bradt, A. G. Evans, D. P. H. Hasselman, and F. F. Lange. Plenum, New York, 1983.
[16]D. B. Marshall and B. R. Lawn, "Residual Stresses in Dynamic Fatigue of Abraded Glass," *J. Am. Ceram. Soc.*, **64** [1] C-6–C-7 (1981).